AN LES STUDY OF UNSTEADY FLOW EVOLUTION IN A SWIRL-STABILIZED INJECTOR WITH EXTERNAL EXCITATIONS

Shanwu Wang, Shih-Yang Hsieh, and Vigor Yang
Department of Mechanical and Nuclear Engineering
The Pennsylvania State University
University Park, PA 16802, USA
shanwu@psu.edu

ABSTRACT

The flow evolution and dynamic response of a gas-turbine swirl-stabilized injector to external forcing were investigated using a large-eddy-simulation (LES) technique. The formulation included the complete conservation equations of mass, momentum, and energy in three dimensions. The numerical scheme employed a density-based, finite-volume approach with explicit time marching. A multi-block technique in conjunction with domain decomposition was implemented to parallelize the code. The anayslsis was first conducted for conditions without external excitations to investigate the internal flow evolution in the injector. Periodical oscillations of the mass flow rate were then imposed at the injector inlet to characterize the injector dynamics over a broad range of frequency. Results indicated that external forcing only exerts minor influences on the mean flow properties due to the broadband characteristics of the injector flow. The dynamic response of the injector, however, depends significantly on the forcing frequency in terms of the acoustic admittance and the mass transfer functions. Energy can be transferred among the various structures in the flowfield under external excitations, consequently causing highly non-uniform distributions of the oscillatory flow properties at the injector outlet. Information of this kind can be effectively used to characterize gas-turbine combustion instability.

INTRODUCTION

Swirl-stabilized injectors have been commonly used in modern gas-turbine engines to achieve efficient clean combustion. In addition to its primary functions of preparing a combustible mixture and stabilizing the flame (Gupta, et al., 1984), an injector acts as a sensitive element that may generate and modulate flow oscillations in the chamber. First, the internal flow evolution in an injector is intrinsically unsteady and involves a wide variety of structures with different time and length scales (Wang et al., 2001). These structures, when convected downstream, can easily interact with the flowfield near the injector exit and change the local flame-zone physicochemistry. Second, the injector flow dynamics dictates the liquid-sheet breakup and droplet formation processes, and subsequently affects the fuel distribution (Lasheras and Hopfinger, 2000). Third, the injector flow may couple resonantly with the acoustic wave in the combustor and lead to large excursions of flow oscillations in the chamber, a phenomenon commonly referred to as combustion instability.

Most of previous studies on gas-turbine combustion instabilities were focused on thermal-acoustic interactions in the chamber. The dynamic behavior of injector was loosely modeled with an acoustic admittance function at the injector boundary, whose specific value is treated as an empirical coefficient. Very limited investigation was conducted into the injector flow dynamics and its response to externally imposed forcing. The present work attempts to remedy this deficiency by developing a comprehensive analysis of the turbulent swirling flow in a contemporary gas-turbine injector. The study employs an LES technique that allows the flowfield to be resolved at a scale sufficient to characterize the injector dynamics. Various flow instability mechanisms and their mutual coupling in the injector are examined is detail under conditions with and without external forcing. The effect of swirl number on the injector dynamics is also studied.

THEORETICAL FORMULATION

A large-eddy-simulation technique is implemented in the present work for turbulence closure, in which large-scale motions are directly simulated, whereas eddies with scales smaller than the grid or filter size are modeled to represent the effects of unresolved motions on resolved scales. The formulation is based on the Favre-filtered conservation equations of mass, momentum, and energy in three dimensions. The equations can be expressed in the following conservative form:

$$\frac{\partial \overline{\rho}}{\partial t} + \frac{\partial \overline{\rho} \tilde{u}_i}{\partial x_i} = 0 \tag{1}$$

$$\frac{\partial \overline{\rho} \tilde{u}_i}{\partial t} + \frac{\partial (\overline{\rho} \tilde{u}_i \tilde{u}_j)}{\partial x_j} = -\frac{\partial \overline{p}}{\partial x_i} + \frac{\partial (\tilde{\tau}_{ij} - \tau_{ij}^{SGS} + D_{ij}^{SGS})}{\partial x_j} \tag{2}$$

$$\frac{\partial \overline{\rho}\tilde{E}}{\partial t} + \frac{\partial[(\overline{\rho}\tilde{E}+\overline{p})\tilde{u}_i]}{\partial x_i} = -\frac{\partial(\tilde{q}_i + \tilde{u}_j\tilde{\tau}_{ij} + Q_i^{SGS} + \sigma_i^{SGS} - H_i^{SGS})}{\partial x_i} \tag{3}$$

where overbar (–) denotes the spatial filter and tilde (~) the Favre-filter, i.e., $\tilde{f} = \overline{\rho f} / \overline{\rho}$. The variables ρ, u_i, p, E, q_i and τ_{ij} represent the density, velocity, pressure, specific total energy, heat flux, and viscous stress, respectively. The subgrid stress, τ_{ij}^{SGS}, and subgrid energy flux, H_i^{SGS}, are treated by means of a compressible-flow version of the Smagorinsky model proposed by Erlebacher et al. (1992). All the other subgrid-scale (SGS) terms in Eqs. (1)-(3), including the SGS viscous diffusion, σ_i^{SGS}, nonlinear viscous stress, D_{ij}^{SGS}, and heat flux, Q_i^{SGS}, were invariably neglected (Martín et al., 1999; Piomelli, 1999). The damping factor recommended by Piomelli et al. (1988) was employed to account for the wall effects on subgrid scales. Details of the filtered equations and the subgrid closure employed have been reported in the cited papers and therefore not presented here for brevity.

The method of characteristics was employed to specify the boundary conditions. The no-slip, adiabatic condition was applied along the solid wall. For a subsonic inflow, the mass flux, total temperature, axial velocity, and flow angle were specified. The pressure was determined using a simplified one-dimensional momentum equation in the direction normal to the inlet. At the outflow boundary, the non-reflecting condition proposed by Poinsot and Lele (1992) was applied. Because the flow was exhausted to the ambient condition after passing through the injector, the surrounding air might be entrained into the computational domain. At the radial boundary, the pressure, total temperature, and axial velocity were specified, and the mass and angular momentum conservation laws were employed to determine the radial and azimuthal velocities, respectively.

NUMERICAL METHED

The theoretical formulation outlined above was solved numerically by means of a density-based, finite-volume methodology. Spatial discretization was achieved using a fourth-order central difference scheme for convective terms along with sixth-order artificial dissipation in generalized coordinates (Rai and Chakravarthy, 1993). Temporal discretization was obtained using a two-step Adam-Bashforth predictor-corrector scheme. A detailed analysis of the numerical accuracy and stability can be found in Wang (2002). A multi-block domain-decomposition method was implemented to facilitate parallel processing in a distributed computing environment using the Massage Passing Interface (MPI) library. The code has been validated by Lu et al. (2003) against a variety of flow problems to establish its credibility. All of the calculations were conducted on an in-house Beowulf system currently consisting of 510 Pentium CPUs.

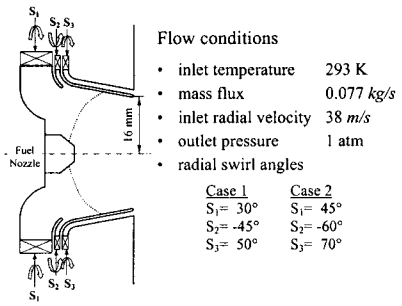

Fig. 1 Schematic diagram of swirl-stabilized injector.

RESULTS AND DISCUSSIONS

The injector under consideration comprises a mixing zone and a fuel nozzle, as shown in Fig. 1. A detailed description is given in Graves (1997). The mixing zone includes a center cylindrical duct, two annular ducts, and three inlet passages corresponding to these ducts, which are spaced radially outward from each other. Three sets of radial air swirlers, denoted as S_1, S_2, and S_3, respectively, are located at the injector entrance. The second swirler is counter-rotating with the others relative to the longitudinal axis. Two different sets of swirl vane angles are considered. The low swirl-number (LSN) case has swirl vane angles of $S_1 = 30°$, $S_2 = -45°$, and $S_3 = 50°$, and the high swirl-number (HSN) case has $S_1 = 50°$, $S_2 = -60°$, and $S_3 = 70°$. The baseline flow condition in the current study included an ambient pressure of 1 atm, an inlet temperature of 293 K, and an inlet mass flow rate of 0.077 kg/s. The Reynolds number based on the diameter and the bulk velocity at the injector outlet is 2×10^5.

The computation domain includes both the injector interior and an external region in the downstream to provide a complete description of the flow development. The length and diameter of the downstream region are 15 and 8 times of the injector diameter, respectively. This region is sufficiently large to minimize the effects of boundary conditions on the injector flow evolution. The numerical grid is carefully chosen such that turbulent length scales in the inertial sub-range of the turbulent kinetic energy (*tke*) spectrum can be properly resolved. The entire grid system has two million points, of which 0.9 million grids are located within the injector. A total of 54 computational blocks are used to facilitate parallel processing.

Unsteady Flow Evolution without External Forcing

Investigation was first conducted into the injector dynamics under conditions without externally imposed forcing. Figures 2 and 3 show the vorticity magnitude contours and the iso-surfaces of the azimuthal velocity, respectively. The flowfields exhibit two salient features as follows. First, as a result of the radial entry of swirling flows, vortex breakdown of the bulb form occurs in the downstream of the centerbody for the LSN case, whereas a much more complex structure prevails for the HSN case. Because of the strong shear between the main flow passage and the central toroidal recirculation zone (CTRZ), a vorticity layer is

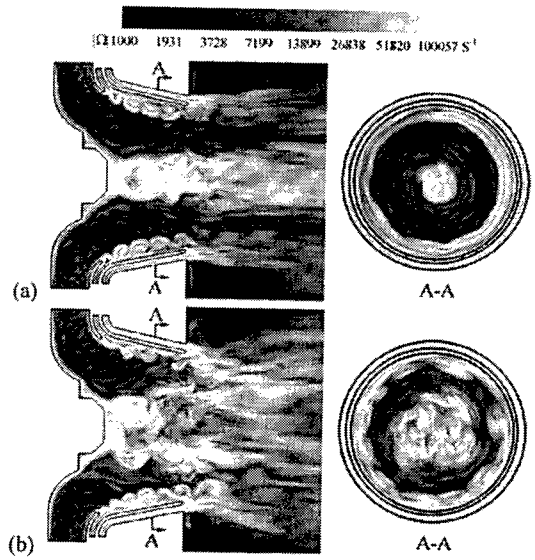

Fig. 2 Snapshots of vorticity magnitude contours, (a) low swirl number and (b) high swirl number.

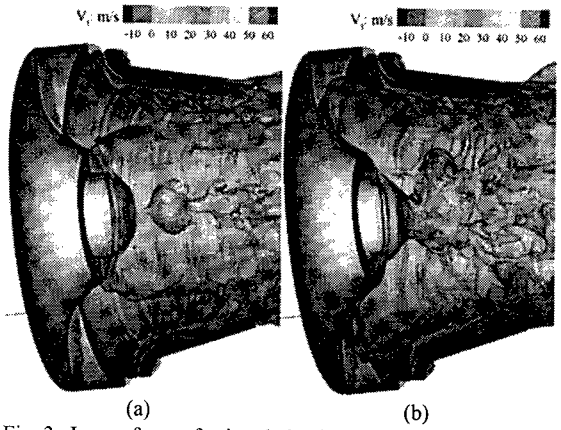

Fig. 3 Iso-surfaces of azimuthal velocity, blue: -10 m/s, yellow, 40m/s, (a) low swirl number and (b) high swirl number.

produced, which subsequently rolls, tilts, stretches, and breaks up into small bulbs, as evidenced in Fig. 2. These vorticity bulbs are then convected downstream and interact with the surrounding flow structures. The second salient feature is the organized vortex shedding from the trailing edge of the guide vane between the first and second flow passages, which originates from the Kelvin-Helmholtz instabilities. Because of the opposition of the swirler vane angles, two counter-rotating flows with different velocities merge at the rim tip and produce a strong shear layer in both the streamwise and azimuthal directions. Vortices are generated and shed downstream sequentially. The ensuing influence on the fuel/air mixing is significant because of the interactions with the thin fuel film on the surface of the guide vane.

The mean axial-velocity field shown in Fig. 4 clearly indicates the existence of a CTRZ (dark region) in the downstream of the centerbody. The axial velocity reaches a

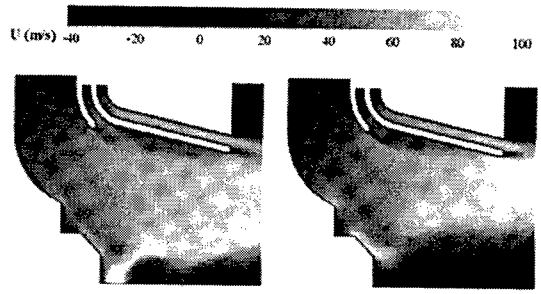

Fig. 4 Contours of time-mean axial velocity, spatially averaged in the azimuthal direction, (a) low swirl number, (b) high swirl number.

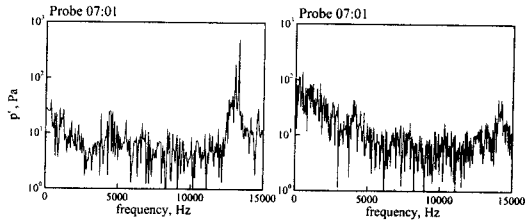

Fig. 5 Frequency spectra of pressure oscillation (x = 9.8, y = 12.5, and z = 0, unit: mm), (a) low swirl number, (b) high swirl number.

large value in that region in the LSN case, but not in the HSN case. This difference in flow topology results from the competition between the centrifugal force and the downward momentum inertia of the incoming flow. The latter has roughly the same magnitude in both cases because of the fixed mass flow rate at the inlet. In the LSN case, the lower azimuthal velocity leads to a weaker centrifugal force. The radial-entry incoming flow can thus penetrate into the center region and results in a low-pressure core near the centerline according to the conservation of angular momentum. On the other hand, the pressure in the wall region is relatively high because of the velocity constraint arising from the no-slip wall condition. Consequently, a strong negative pressure gradient is generated in the axial direction and causes a wall-jet effect along the centerline, which then leads to a rapid flow acceleration. (Wang, 2002)

Figure 5 shows the prevalence of a dominant harmonic at 13000 Hz in the LSN case, resulting from the vortex shedding from the trailing edge of the guide vane. In the HSN case, three harmonics at 14000, 4000, and 1500 and Hz exist due to the shear layer downstream of the guide vane, the central recirculation flow, and their interaction/competition, respectively. (Wang, et al., 2002)

Unsteady Flow Evolution with External Forcing

The dynamic response of the injector to external forcing was investigated by imposing periodical oscillations of the mass flow rate at the injector entrance.

$$\dot{m} = \dot{m}_0 \left[1 + \alpha \sin(2\pi f_F t)\right] \tag{4}$$

where $\dot{m}_0$ and f_F denote the mean mass flow rate and the external forcing frequency, respectively. The amplitude of oscillation, α, is fixed at 10% in the present study. The forcing frequency covers a range from 400 to 13000 Hz due to the broadband nature of the injector flow dynamics.

A triple decomposition method developed by Apte and Yang (2002) was used for data analysis. The method extended the approach of Hussain and Reynolds (1970) for incompressible flows to include compressibility effects using the Favre-averaged ensemble-averaging and time-averaging techniques given below:

$$\tilde{u}(x,t) = \bar{\tilde{u}}(x) + u'(x,t) = \bar{\tilde{u}}(x) + u^{a}(x,t) + u''(x,t) \qquad (5)$$

where $\bar{(\cdot)}^{\leftrightarrow}$ represents the density-weighted long time average and $(\,)'$ the fluctuation. The latter is further decomposed into the density-weighted phase averaged oscillation, $(\,)^{a}$, and turbulent fluctuation, $(\,)''$.

Figure 6 shows the magnitude of the vorticity fluctuation under external forcing at f_F = 13000 Hz for the HSN case, obtained by subtracting the long-time averaged quantity from the instantaneous value. Well-organized structures appear in the forward section of the injector and are convected downstream with the local flow velocity. The result also reveals another interesting phenomenon about the energy distribution. External forcing tends to redistribute the vorticity and renders a more uniform field. The vorticity and its associated flow energy are usually strengthened in the forward section of the injector, but become weakened near the boundary of the CTRZ. Two mechanisms are identified to account for this phenomenon. First, the inlet flow oscillation results in a well-defined vortical wave; the vorticity field in the forward section is hence strengthened. Second, the high frequency forcing helps breakup the large flow structures, and enhances the energy transfer from low-frequency/large-scale motions to high-frequency/small-scale motions by means of an additional pathway to transfer energy between the mean flowfield and turbulent motions. (Brereton et al., 1990; Apte and Yang, 2002; Wang, 2002)

Figure 7 shows the mean axial velocity fields under conditions with and without external forcing. No discernible difference was observed. A similar result is observed for the turbulent kinetic energy, as evidenced in Fig. 8. High

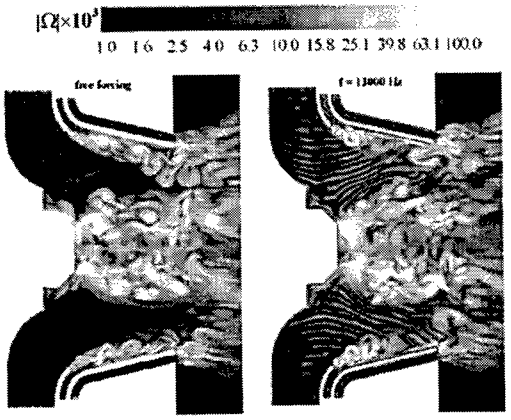

(a) (b)

Fig. 6 Snapshots of vorticity-fluctuation magnitude: (a) without forcing and (b) with forcing; HSN case

turbulent intensity appears in the downstream of the centerbody, where the central recirculation flow appears, and in downstream of the guide vane, where the vortex shedding prevails. The modification of the intensity near the end of the centerbody suggests a change of the dynamic flow pattern.

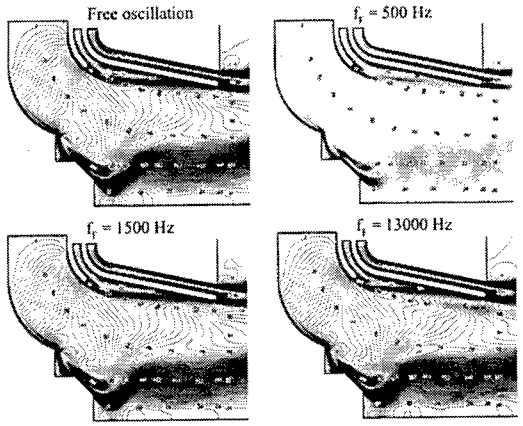

Fig. 7 Contours of time-mean axial velocity, spatially averaged in the azimuthal direction; HSN case.

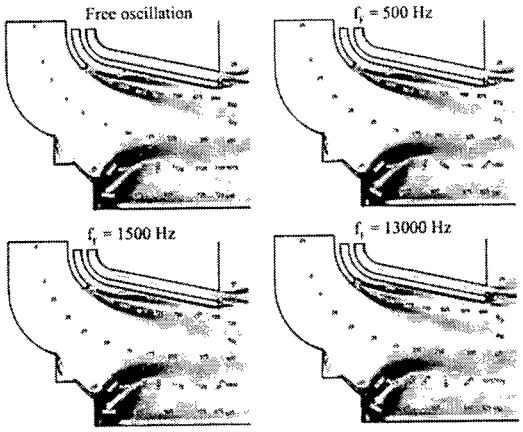

Fig. 8 Contours of turbulence kinetic energy, spatially averaged in the azimuthal direction; HSN case

Although there exist some minor differences in the mean flowfield under different external excitations, the turbulent properties appear to be identical from the global viewpoint. This may be attributed to the weak forcing relative the flow intensity. The broadband nature of the injector flow also discourages the modulation of the mean flow by a single-harmonic excitation unless that frequency happens to cause resonance of the local flow structure in the injector. (Brereton et al., 1990)

Figures 9 shows the frequency spectra of pressure oscillations under 500, 1500, and 4000 Hz forcing. Compared to the free-forcing case, a dominant harmonic corresponding to the forcing frequency is clearly observed. The excitation usually has minor effects on the spectral contents away from the forcing frequency except for f_F = 1500Hz, which also leads to the maximum pressure oscillation among the four cases considered herein.

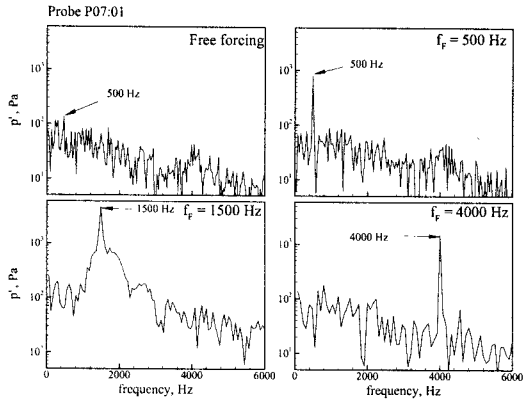

Fig. 9 Frequency spectra of pressure oscillations at x = 9.8 mm, y = 12.5 mm, and z = 0 mm; HSN case

The dynamic behavior of the injector can be best characterized by an acoustic admittance and mass transfer functions at the outlet. Following common practice, the acoustic admittance function, A, is defined as

$$A(f_F) = \frac{\hat{u}'' / \overline{a}}{\hat{p}'' / \gamma \overline{P}} \tag{6}$$

where $\overline{a}$ and $\overline{P}$ denote the mean speed of sound and mean static pressure, respectively. The hat $\hat{(\,)}$ represents the Fourier component at the forcing frequency.

Figure 10 shows the radial distribution of the admittance function at the injector exit for four different forcing frequencies, *i.e.*, 500, 900, 1500, and 4000 Hz. The admittance function reaches its maximum at the forcing frequency of 500 Hz, especially near the upper boundary where the breakup of the liquid film occurs in practice. A small pressure oscillation at 500 Hz may result in a large excursion of velocity fluctuation, which consequently exerts a strong influence on the spray formation process in that region.

Another important measure of the injector response is the mass transfer function defined as follows

$$T(f_F) = \frac{\hat{\dot{m}}''^{a}_{out} \cdot A_{out}}{\hat{\dot{m}}''^{a}_{in} \cdot A_{in}} \tag{7}$$

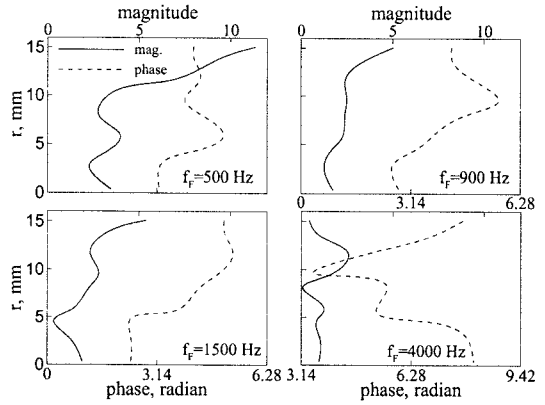

Fig. 10 Acoustic admittance functions at injector outlet for 500, 900, 1500, and 4000 Hz external excitations; HSN case.

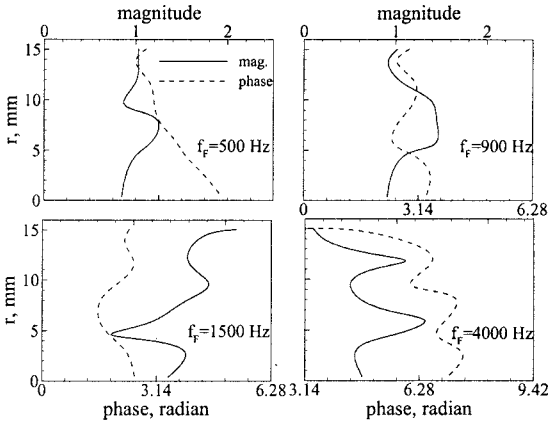

Fig. 11 Transfer functions of injector mass flux; HSN case

where $\dot{m}''_{(\cdot)}$ and A represent the mass flux and the cross-sectional area, respectively. The subscripts *in* and *out* denote the injector inlet and outlet, respectively.

The mass flux transfer function shown in Fig. 11 clearly indicates that the mass flux oscillation is significantly modulated by the external excitation. For the 500 Hz forcing, the distribution is almost uniform in the range of 0.85 ~ 1.23. However, the magnitude is greater than 2 near the upper boundary for f_F = 1500 Hz. This phenomenon suggests that the 1500 Hz forcing enhances the flow oscillation near the upper boundary where the intrinsic frequency of the flow structure has the same value. The 1500 Hz flow motion is considered as a consequence of the competition between the central recirculation flow and the vortex shedding from the trailing edge of the guide vane (Wang et al., 2002). An external excitation at this frequency modulates the local flow evolution, and subsequently changes the effective flow passage area at the injector exit.

Figure 12 shows the transfer function of the total injector mass flow rate at the exit, defined as

$$M(f_F) = \frac{\hat{\dot{m}}''_{out}}{\hat{\dot{m}}''_{in}}. \tag{8}$$

The oscillations of the mass flow rates at the inlet and the outlet are almost in-phase at f_F = 500 Hz. A phase shift is, however, observed when the forcing frequency is 1500 Hz or higher due to the compressibility effects. This phenomenon can be examined using a characteristic frequency analysis based on the injector flow condition. Assume the streamwise length from the injector inlet to the outlet is $L \approx 30$ mm and the speed of sound $\overline{a} \approx 340$ m/s , then the phase difference, θ, of a traveling acoustic wave between the inlet and the outlet is

$$\theta \approx 2\pi L f_F / \overline{a} = 2\pi f_F / f_L \tag{9}$$

where the acoustic characteristic frequency, f_L, is given by

$$f_L = \overline{a} / L \approx 11{,}000 Hz .$$

Figure 12 shows good agreement between the above analysis, Eq. (9), and the numerical simulation, Eq. (8). The oscillation of the mass flow rate propagates in the form of acoustic wave. The magnitude of the mass flow-rate transfer function

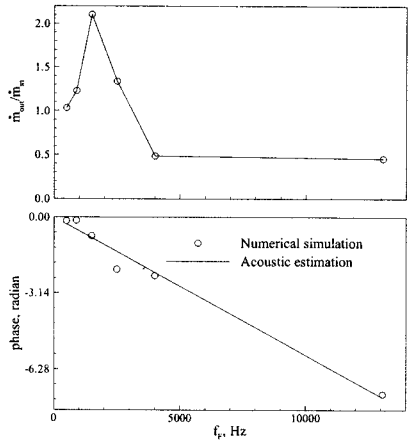

Fig. 12 Transfer functions of total injector mass flow rate; (a) magnitude and (b) phase.

achieves its maximum at f_F = 1500 Hz as expected. In the present simulation, the mean mass flow rate is well conserved. A large disparity of the mass flow rate between the inlet and outlet, however, is clearly observed in the instantaneous flowfield, especially at the 1500 Hz forcing. The flowfield is considerably excited at this frequency, at the expense of suppressing motions at other frequencies. In summary, the forcing frequency affects not only the spatial distribution of the mass flux fluctuation as shown in Fig. 11, but also the oscillation of the overall mass flow rate, as evidenced in Fig. 12.

CONCLUSIONS

A comprehensive numerical analysis has been conducted to investigate the internal flow evolution and dynamic response of a swirl-stabilized injector under conditions with and without external forcing. The formulation treated the unsteady, three-dimensional conservation equations of mass, momentum, and energy, with turbulence closure achieved using an LES technique. Detailed injector flow dynamics was studied systematically over a broad range of forcing frequency. Results indicate that the effects of externally imposed oscillations on the mean flow and turbulence properties appear to be quite small due to the broadband nature of the injector flowfield. External forcing, however, may exert substantial influences on the injector response in terms of the acoustic admittance and mass transfer function. Significant flow modulation occurs if the forcing frequency matches with the intrinsic frequencies of local flow structures. Energy can always be transferred from the non-resonant modes to the resonant modes, thereby causing large excursions of flow oscillations, both spatially and temporally.

ACKNOWLEDGEMENTS

This work was sponsored by the NASA Glenn Research Center under Grant NAG 3-2151. The support and encouragement of Kevin Breisacher is greatly appreciated.

REFERENCES

Apte, S. and Yang, V., 2002, "Unsteady Flow Evolution in Porous Chamber with Surface Mass Injection, Part 2: Acoustic Excitation," *AIAA J.*, Vol. 40, pp. 244-254.

Brereton, G.J., Reynolds, W.C., and Jayaraman, R., 1990, "Response of a Turbulent Boundary Layer to Sinusoidal Free-Stream Unsteadiness," *J. Fluid Mech.*, Vol. 221, pp. 131-159.

Erlebacher, G., Hussaini, M. Y., Speziale, C. G., and Zang, T. A., 1992, "Toward the Large Eddy Simulation of Compressible Turbulent Flows," *J. Fluid Mech.*, Vol. 238, pp. 155-185.

Graves, C.B., 1997, "Outer Share Layer Swirl Mixer for a Combustor," US Patent 5-603-211.

Gupta, A.K., Lilley, D.G., and Syred, N., 1984, "Swirl Flows," Abacus Press.

Hussain, A.K.M.F. and Reynolds, W.C., 1970, "The Mechanics of Organized Wave in Turbulent Shear Flow," *J. Fluid Mech.*, Vol. 41, pp. 241-258.

Lasheras J.C. and Hopfinger E.J., 2000, "Liquid Jet Instability and Atomization in a Coaxial Gas Stream," *Annu. Rev. Fluid Mech.*, Vol. 32, pp 275-308.

Lu, X., Wang, S., Sung, H., Hsieh, S.Y., and Yang, V., 2003 "Large Eddy Simulation of Turbulent Swirling Flows Injected into a Dump Chamber," submit to *Phys. Fluids.*

Martín, M. P., Piomelli, U., and Candler, G. V., 1999, "A Priori Test of SGS Models in Compressible Turbulence," *Proceedings of the 3rd ASME/JSME Joint Fluid Engineering Conference*, San Francisco, California, USA, *FEDSM* 99-7313.

Piomelli, U., Moin, P., and Ferziger, J. H., 1988, "Model Consistency in Large Eddy Simulation of Turbulent Channel Flows," *Phys. Fluids*, Vol. 31, pp. 1884-1891.

Poinsot, T. J. and Lele, S. K., 1992, "Boundary Conditions for Direct Simulations of Compressible Viscous Flows," *J. Comp. Phys.*, Vol. 101, pp. 104-129.

Rai, M. M. and Chakravarthy, S., 1993, "Conservative High-Order Accurate Finite Difference Method for Curvilinear Grids," AIAA Paper 93-3380.

Wang, S., Hsieh, S.Y., and Yang, V., 2001, "Numerical Simulation of Gas Turbine Swirl-Stabilized Injector Dynamics," AIAA Paper 2001-0334.

Wang, S., Hsieh, S.Y., and Yang, V., 2002, "Vortical Dynamics and Acoustic Response in Gas-Turbine Swirl-Stabilized Injectors," AIAA Paper 2002-1008.

Wang, S., 2002, "Vortical Flow Dynamics and Acoustic Response of Gas-Turbine Swirl-Stabilized Injector," Ph.D. Thesis, The Pennsylvania State University, University Park, PA, USA.